J. Fluid Mech. (2007), *vol.* 590, *pp.* 355–380.
doi:10.1017/S0022112007008063 Printed in the United Kingdom

An experimental investigation on the interaction of hydraulic jumps formed by two normal impinging circular liquid jets

R. P. KATE, P. K. DAS AND SUMAN CHAKRABORTY

Department of Mechanical Engineeringx Indian Institute of Technology, Kharagpur – 721302, India

(Received 31 October 2006 and in revised form 25 June 2007)

The flow field due to two normal impinging liquid jets is different from the flow field associated with a single normal impinging liquid jet, and even from the flow field around two normal impinging compressible fluid jets. Depending on the spacing between the two jets and their relative strengths, different kinds of hydraulic jump interactions are possible, resulting in a variety of flow patterns. The present study experimentally elucidates the jump–jump interactions formed in such cases, for different values of inter-jet spacings and for different strengths of the individual jets. Analogous flow fields associated with the interactions between a single impinging jet and a fence are also studied to allow convenient experimental flow vizualizations.

1. Introduction

1.1. *Single impinging liquid jet*

Impingement cooling is a mechanism of heat transfer by means of collision, and can be achieved when a fluid jet strikes a surface. Around the impingement region, the boundary layer is very thin, and hence heat can be transferred easily (Lienhard 2006). If the colliding fluid is a liquid, the flow of the thin film often gives rise to the formation of a 'hydraulic jump'.

Various fluid dynamic aspects of hydraulic jumps, formed as a consequence of the interaction between a single jet and a target plate (see figure 1 for schematic and experimental vizualization), have been investigated. Early efforts were devoted to the study of hydraulic jumps with circular profiles, which are usually formed as a result of the normal impingement of a single circular liquid jet (Watson 1964; Olsson & Turkdogan 1966; Ishigai *et al.* 1977; Nakoryakov, Pokusaev & Troyan 1978; Craik *et al.* 1981; Bohr, Dimon & Putkaradze 1993; Godwin 1993; Liu & LIenhard 1993*a*, *b*; Higuera 1994, 1997; Blackford 1996; Hansen *et al.* 1997; Brechet & Néda 1999; Yokoi & Xiao 2002; Bush & Arisstoff 2003). In some carefully controlled experiments, hydraulic jumps of different non-circular geometries have also been observed due to the normal impingement of circular liquid jets on horizontal plates (Ellegaard *et al.* 1998, 1999; Aristoff *et al.* 2004; Bush, Aristoff & Hosoi 2006). In comparison to normal impinging jets, oblique impinging jets have received less attention (Beltos 1976; Rubel 1981, 1982; Sparrow & Lovell 1980; Stevens & Webb 1991; Tong 2003). Recently, Kate, Das & Chakraborty (2007*a*, *b*) studied the formation of hydraulic jumps due to oblique impingement of circular liquid jets, elucidating the formation of several interesting and non-intuitive fluid flow patterns.

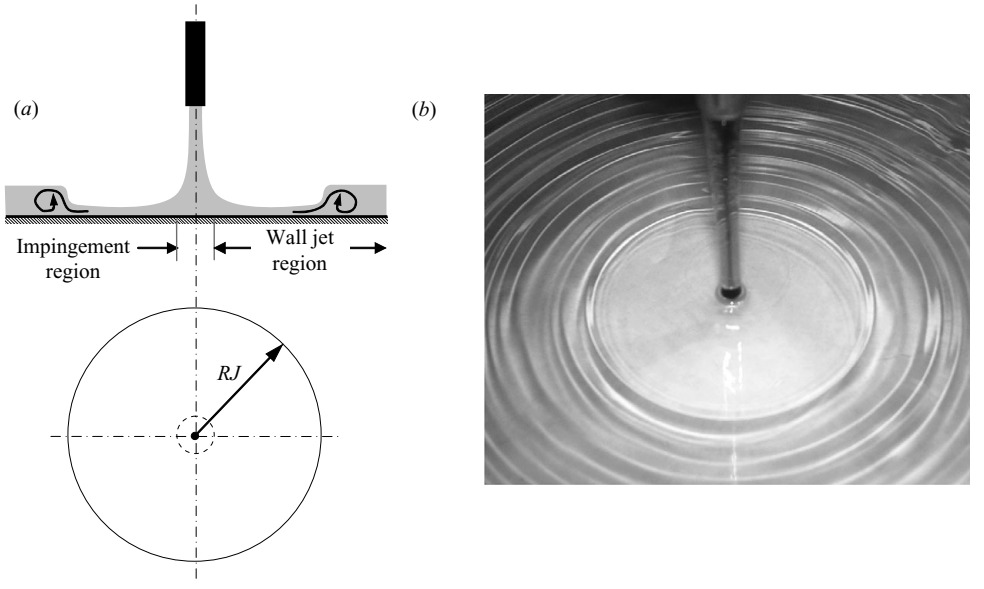

FIGURE 1. (*a*) Schematic of a normal impinging jet showing various flow regions; (*b*) a circular hydraulic jump in laboratory experiments.

1.2. *Multiple impinging jets*

Though very high heat transfer rates can be achieved in the vicinity of the stagnation point (or impingement point region) with a single jet in impingement cooling, the heat transfer rate decreases sharply as the distance from the stagnation point increases. As a result, the net heat flux distribution is highly non-uniform around the stagnation point. To overcome this limitation, in many industrial applications, multiple impinging jets are used (Thielen, Jonker & Hanjalic 2003; Hamed & Akmal 2005). In practice, the cooling performance obtained by employing multiple impinging jets is greatly improved, since it strengthens the protection of surfaces subjected to strong thermal gradients. Such improvements obtaining motivates improved scientific understanding of the fluid dynamic process that dictates the associated transport mechanisms.

Most studies on twin impinging jets have been on air (or a compressible fluid) jets. Following the studies of Siclari, Migdal & Luzzi (1976), Siclari *et al.* (1977), Siclari, Hill & Jenkins (1981), Hill & Jenkins (1980), Saripalli (1983), Hill (1985), Gilbert (1989), Miller (1995), Barata (1996), and Cabrita, Saddington & Knowles (2005), it can be inferred that the flow due to twin impinging jets, in general, is characterized by the following distinct regions (see figure 2):

1. Lift jet flow or free jet flow
2. Jet impingement region
3. Inner wall jet region
4. Outer wall jet region
5. Fountain formation region
6. Fountain upwash flow region, and
7. Entrainment

The important characteristics of two-jet impingement flows are the fountain upwash flow produced by the colliding wall jets, and entrainment of ambient air into different regions of the flow (Saripalli 1983). The first two regions are similar to that of single jet impingement flow. Opposite walls from the two jets jets collide and form

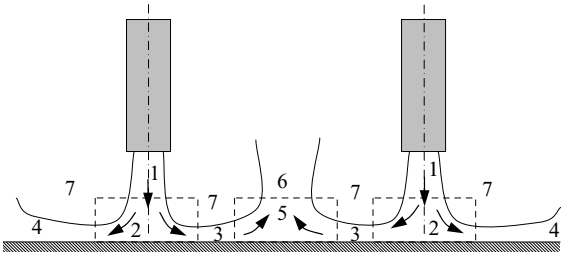

FIGURE 2. Schematic of flow formed by two impinging jets of compressible fluid: 1. free jet flow, 2. jet impingement region, 3. inner wall jet region, 4. outer wall jet region, 5. fountain formation region, 6. fountain upwash flow, 7. entrainment.

a stagnation or upwash deflection region (Siclari *et al.* 1981). The fountain, located midway between the nozzles, moves upward and spreads spatially by entraining the surrounding fluid (Saripalli 1983). Air entrained by the two jets causes a sub-atmospheric region between the two nozzles and there is an attraction between the two jets, causing their axes to curve and eventually merge, forming a single jet (Elbanna & Sabbagh 1989). If the upwash flow comes close to the free jet, a recirculation of the upwash flow can occur (Siclari *et al.* 1981); this has been visualized experimentally by several investigators (Siclari *et al.* 1997; Adarkar & Hall 1969). The fountain formation region, and fountain upwash flow, which are typical of twin impinging jets, are briefly described in the following discussions.

1.2.1. *Fountain formation region and the stagnation line*

Upon the collision of the wall jets, a fountain formation zone, accompanied by a stagnation spot between the two jets, appears. In this stagnation spot, there is a stagnation line along the collision zone. The location where the inner wall jets due to the adjacent nozzles meet or collide is termed as the 'stagnation line'. The characteristics of a stagnation line depend on the relative strength (momentum) of the individual jets. If the two vertical jets impinge on a flat horizontal surface with equal momentum, the stagnation line will be a straight line everywhere, equidistant from the two-jet impingement centres. If the two jets have unequal momentum (due to unequal diameters or exit velocity, for example) or are inclined at an angle other than 90° relative to the horizontal surface, the stagnation line will, in general, exhibit a curvature. Its position shifts towards the weaker jet and its curvature increases as the ratio of the jet momenta is decreased (Siclari *et al.* 1981). It has been shown experimentally that for a pair of two-dimensional colliding wall jets, the location of the stagnation region approximately corresponds to the position of an equal maximum total pressure in each wall jet layer (Kind & Suthanthiran 1972). For vertical jets of equal momentum, the stagnation line location is given as (Siclari *et al.* 1981)

$$\frac{r_2}{r_1} = \left(\frac{V_2}{V_1}\right)\left(\frac{d_2}{d_1}\right) \tag{1.1}$$

where r_1 and r_2 are the radial distances of the stagnation line from impingement points of jets 1 and 2, V_1 and V_2 are the jet velocities, and d_1 and d_2 are the jet diameters.

1.2.2. *Upwash fountain flow region*

At the stagnation line location, the opposing wall jets merge and accelerate to form a fan-shaped upwash. The direction and strength of the upwash fountain flow is

strongly dependent on the strength of the parent jets and their relative orientations, assuming a uniform impingement surface. The upwash fountain moves upwards and spreads spatially by entraining the surrounding air. When the two jets have equal momentum, the fountain flow is vertical and centred. However, in the case of unequal momentum, the fountain is inclined towards the weaker jet and its angle increases with increasing difference in the jet momentum (Saripalli 1983). At each point in the upwash sheet along the path of the stagnation line, the upwash generally exhibits large three-dimensional flow structures. Far from the impingement centres of the jets, the upwash inclination tends to become tangential to the impingement plane (Siclari *et al.* 1981). The fountain flow is known to involve complex flow structures; it has growth rates considerably larger than the growth rates found in free plane jets, and turbulent mixing rates are considerably higher in upwash flows than in other free turbulent flows (Hill 1985). The fountain is quite sensitive to small imbalances between the jets and appears to be unstable under certain conditions (Cabrita *et al.* 2005; Skifstad 1970).

An extensive review of the existing literature on twin impinging jets reveals that that a most of the applications deal with the vertical take-off-and-landing (VTOL) aircraft. These aircraft are equipped with powered lift jets and have complicated flow fields, while hovering in proximity with the ground. The flow fields are typically characterized by a fountain upwash produced by the colliding wall jets and the entrainment of ambient air into the flow, which strongly influence the lift force on the aircraft. Also, the exhaust flow from the fountain often causes an elevation in the skin temperature, resulting in a degradation of the propulsion system performance. Despite such significant consequences, the hydraulic jump interactions of twin impinging jets, interacting over a wide range of inter-jet spacings, are yet to be reported in the literature. The aim of the present work, therefore, is to investigate experimentally the flow field due to two normal impinging jets, with the primary intention of elucidating the mechanism of the associated hydraulic jump interactions. The outline of the remaining part of this paper, is as follows. In § 2, experimental facility for two normal impinging liquid jets is discussed. In § 3 and § 4, the flow field due to two normal impinging liquid jets is described, both for distant and adjacent impinging jets (covering hydraulic jump interactions due to equal impinging jets), while an experimental simulation of the flow due to two equal jets using a single jet and a fence is described in § 5. Upwash fountain flow is described in § 6. Effects of jump interactions on jump profiles are described § 7. Jump interactions for unequal jets are described in § 8 and in § 9 concluding remarks based on the present study are outlined.

2. Description of the experimental facility

The experimental set-up employed for the present study primarily consists of a closed-loop water jet system comprising centrifugal pumps, rotameters and jet-issuing nozzles. The details of the experimental facility can be found in Kate *et al.* (2007*a*), and are omitted here for the sake of brevity. The original set-up is slightly modified to incorporate two independent closed-loop water jet systems, instead of a single one. The upper and the lower limits of the volume flow rates of the liquid (Q_{large} and Q_{small}, respectively) are controlled by using bypass valve arrangements. The film thickness at the point of intersection of the stagnation line with the line joining the impingement points of the two jets is measured using a needle contact type conductivity probe. The film thickness is estimated from the probe response using a calibration curve. To verify the correctness of the measured variables, experiments are conducted using a

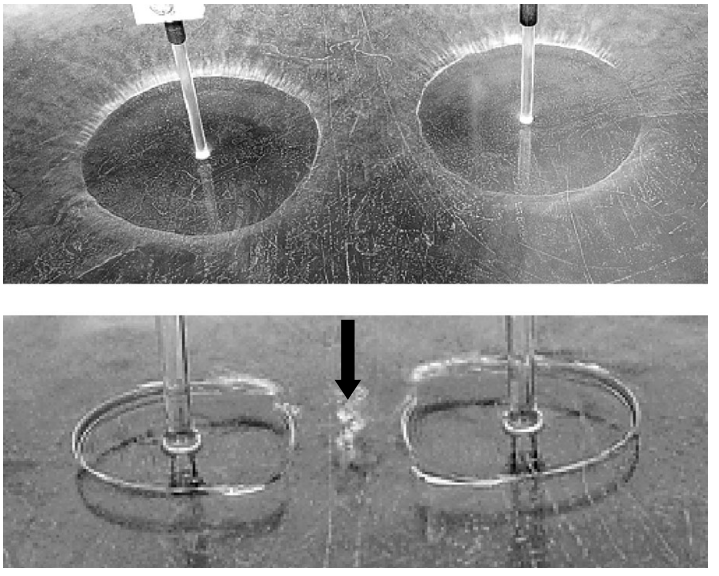

FIGURE 3. (*a*) Two far-distant impinging jets indicating no jump interactions. (*b*) Two jets spaced at a critical distance, volume flow rate $Q = 1.25 \times 10^{-5}\ \mathrm{m^3\,s^{-1}}$, $S/D = 11$ (where S is the inter jet spacing and D is the jet diameter), $H/D = 14.4$ (where H is the drop height). Interaction is visible (indicated with an arrow) at the stagnation line (or line of partition).

single jet to create a circular hydraulic jump. Jump radius (Kate *et al.* 2007*a*) and film thickness data obtained from these experiments closely agree with those reported by Arakeri & Rao (1996), and Rao & Arakeri (1998).

3. Description of the phenomenon

In the present study, the impinging jets are termed 'jets of equal strength' or 'equal jets' when the nozzle diameters and the jet velocities of both the jets are the same, and 'jets of unequal strength' or 'unequal jets' when nozzle diameters and/or the jet velocities are not the same.

From our flow vizualization experiments, it has been observed that the flow field due to two impinging jets, for a given volume flow rate of liquid, mainly depends on the spacing (S) between the two jets. When two jets are spaced at too large a distance, the radial symmetry of the circular hydraulic jump remains unaffected, indicating no perceptible interaction between the hydraulic jumps, as can be seen if figure 3(*a*). Below a threshold inter-jet spacing (S_c), the hydraulic jumps of individual jets start interacting with each other, disturbing of the radial symmetry of the individual jump profiles. This critical spacing (S_c) is observed to be a function of the volume flow rate of liquid (Q) through each jet, as evident from figure 4. In general, the system of two impinging jets can be broadly grouped into three categories: (a) far-distant, (b) distant, and (c) adjacent.

'Far-distant' when the spacing between the two jets is greater than the critical spacing for a given volume flow rate of liquid. 'Distant' is when the spacing between the two jets is less than the critical spacing, but is greater than R, where $R \approx (RJ_1 + RJ_2)/2$ and RJ_1, RJ_2 are the radii of the circular hydraulic jumps formed by two jets independently, for a given volume flow rate of liquid. 'Adjacent' impinging jets are spaced at a distance less than R. The classification of the two-jet system is summarized

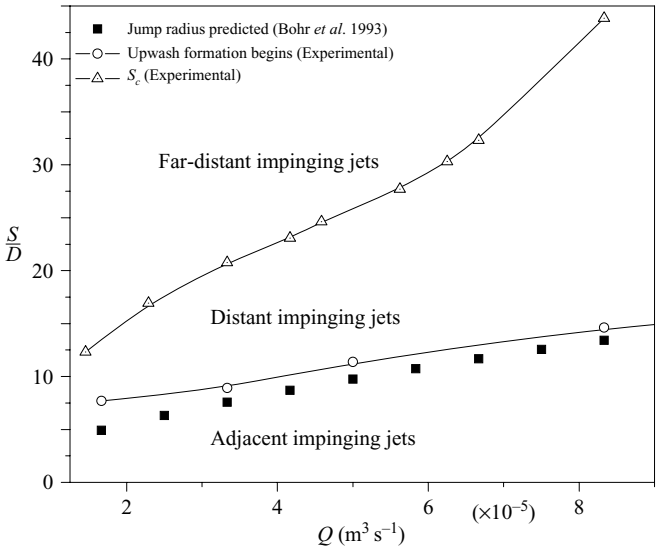

FIGURE 4. Types of two-jet impingement systems.

System of two jets	Jet spacing	Jump interaction
Far-distant	$S > S_c$	negligible interaction
Distant	$S_c > S \gg R$	thick film interaction
Adjacent	$S \leqslant R$	thin film interaction

TABLE 1. Classification of two impinging jets.

in table 1, while typical plots defining the distant and the adjacent impinging jets are depicted in figure 4. The wall jet interactions have distinct effects on the radial symmetry of the circular hydraulic jumps. The resulting jump profiles are dictated by the types of interaction that the opposing wall jets have. This, in turn, depends on the spacing between the jets and their relative strength. These interactions are described for two equal and unequal jets in the following sections.

4. Equal jets

4.1. *Far-distant and distant jets*

Two far-distant impinging jets are depicted in figure 3(*a*): the circular hydraulic jump profiles remain more or less intact in such cases. However, for distant impinging jets, a region of stagnation line is clearly visible, as can be seen in figure 3(*b*). In such cases, the hydraulic jumps interact to form thick films. Theses interactions are relatively weak and do not have significant effects on the radial symmetry of the circular hydraulic jumps.

A schematic diagram of two distant impinging jets describing various flow field regions is depicted in figure 5(*a*), while the corresponding flow patterns, as observed during our laboratory experiments are depicted in figure 5(*b*). It can be seen from figure 5(*a*) that the radial wall jets, in the forms of thick films in the downstream regions of the jumps, butt against each other at the stagnation line. At the stagnation

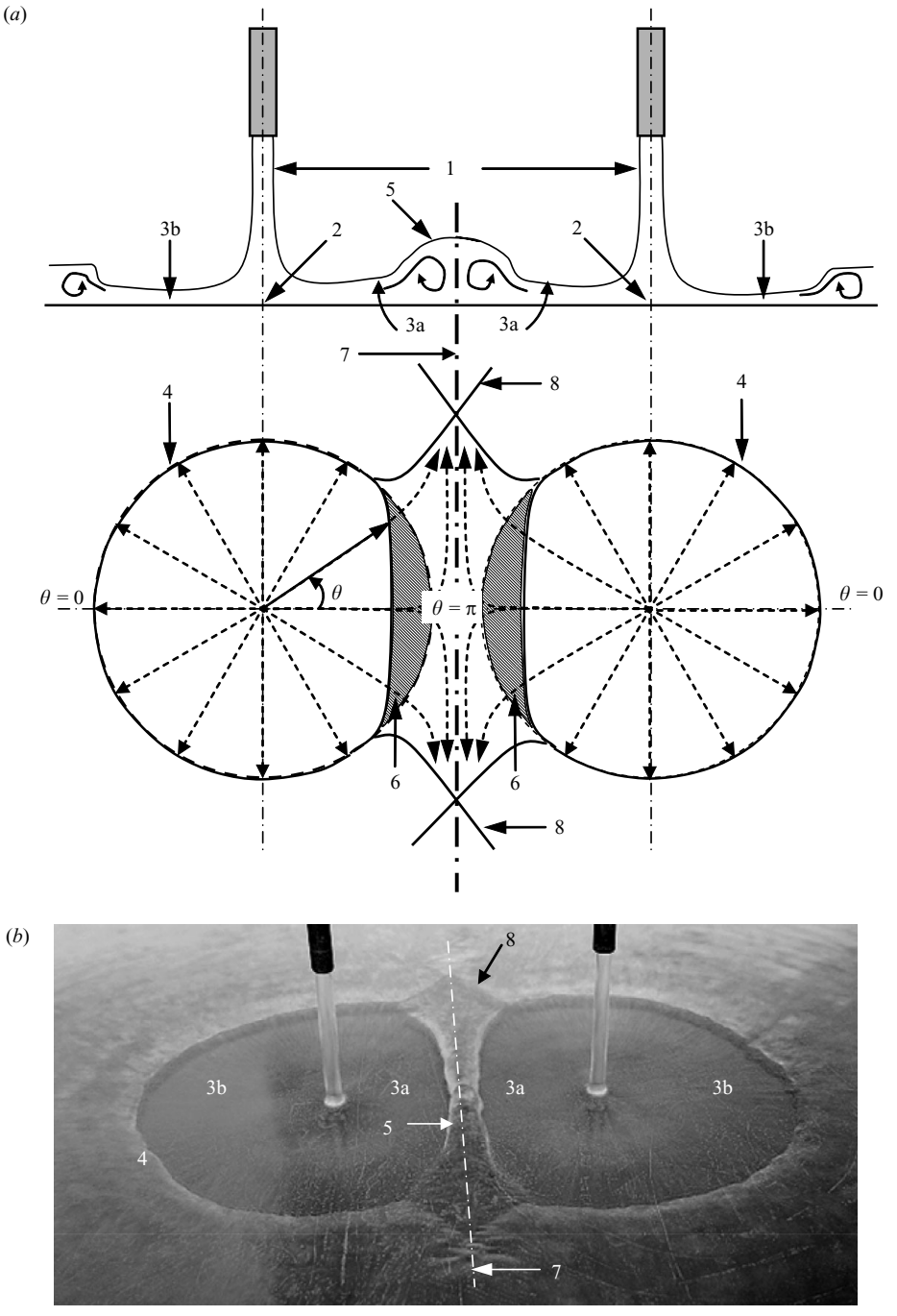

FIGURE 5. (*a*) Schematic of two distant impinging jets showing major flow regions (*b*) Hydraulic jump interactions in adjacent impinging jets observed during laboratory experiments ($Q = 8.33 \times 10^{-5}$ m^3 s^{-1}, $S/D = 15.4$, $H/D = 10$). 1. Free jet region, 2. Impingement region, 3a. Inner wall jet regions, 3b Outer wall jet regions, 4. Fountain formation region, 5. Up-wash flow, 6. Stagnation line, 7. Hydraulic jump, 8. Interacting jump segments.

line, the radially spreading streams change direction and become almost parallel to the stagnation line. However, water streams coming from each of the jet do not mix even at the stagnation line and retain their identity along this line till drainage takes place at the periphery of the target plate. This has clearly been revealed using jets of different colours. The direct impact between the opposing streams of fluid results in an increase in film thickness of the wall jet after the jump, conferring a typical 'dome' shape to the stagnation line region. The increase in the film thickness in the inner wall jet region downstream of the jumps has a significant consequence for corresponding jump locations. Bohr *et al.* (1993), in their experimental studies on circular hydraulic jumps, observed similar inter-dependence between the jump radius and the downstream film thickness. They observed that as the height of the ring controlling the film thickness after the jump increases, the jump becomes stronger and its radius decreases. This can explain the nature of the non-circular hydraulic jumps observed in the present study as well. In the present case, unification of the opposing radial streams at the stagnation line results in a small dome-shaped region along the stagnation line.

The thickness of the film (h) is uneven, being maximum at the centre of the stagnation line (h_π at radial location $\theta = \pi$). The film thickness gradually decreases in both directions along the stagnation line. The film thickness at an opposite radial location (h_0 at radial location $\theta = 0$) remains unaltered. The hydraulic jump at $\theta = \pi$ is observed to be the strongest, which corresponds to the centre of the stagnation line, where the film thickness after the jump is the maximum. At the same location, the distance of the jump from the impingement point is a minimum. The outer wall jet regions (both before and after the jump), however, remain similar to those due to an independent single impinging jet. The corresponding jump profiles are, therefore, unaffected and are circular segments. The radial location of the jump at $\theta = 0$ is equal to the radius of the circular hydraulic jump formed due to a single independent jet.

The effect of jet spacing (keeping Q fixed) on the film thickness at the centre of the stagnation line, and the corresponding jump location is depicted in figures 6(a) and 6(b), while the effect of volume flow rate (keeping S fixed) on film thickness at the centre of the stagnation line and the corresponding jump location is depicted in figure 6(c). As can be seen from these figures, the ratio h_0/h_π is always greater than or equal to 1. It decreases with increase in S, or decrease in Q. Accordingly, the ratio RJ_0/RJ_π (where RJ_0 and RJ_π are the radial locations of the jump at $\theta = 0$ and $\theta = \pi$ respectively) is always less than or equal to 1. It increases with increase in S (keeping Q fixed) or decrease in Q (keeping S fixed), as can be seen from figures 6(a), 6(b) and 6(c), respectively.

The above-mentioned radial-unidirectional flow has an interesting effect on the section of the hydraulic jump corresponding to a radial location that is far away from the centre of the stagnation line. The flow along the stagnation line, in effect, displaces the radial segments (refer to region 8 in figure 5) of the hydraulic jump at that location. The two jump segments eventually result in obliquely intersecting hydraulic jumps. These jump–jump interactions impart in a typical 'butterfly-shape' to the collective jump profile, as evident from figures 5(a) and 5(b). Similar jump–jump interactions (due to obliquely impinging single circular liquid jets) are discussed in detail in Kate *et al.* (2007a, b). The butterfly-shape jump profiles, as obtained from the present experiments, are depicted in figure 7. The hydraulic jump profile, corresponding to a single normally impinging jet, as obtained from the analysis of Bohr *et al.* (1993), is superimposed. A reasonably good agreement between the two

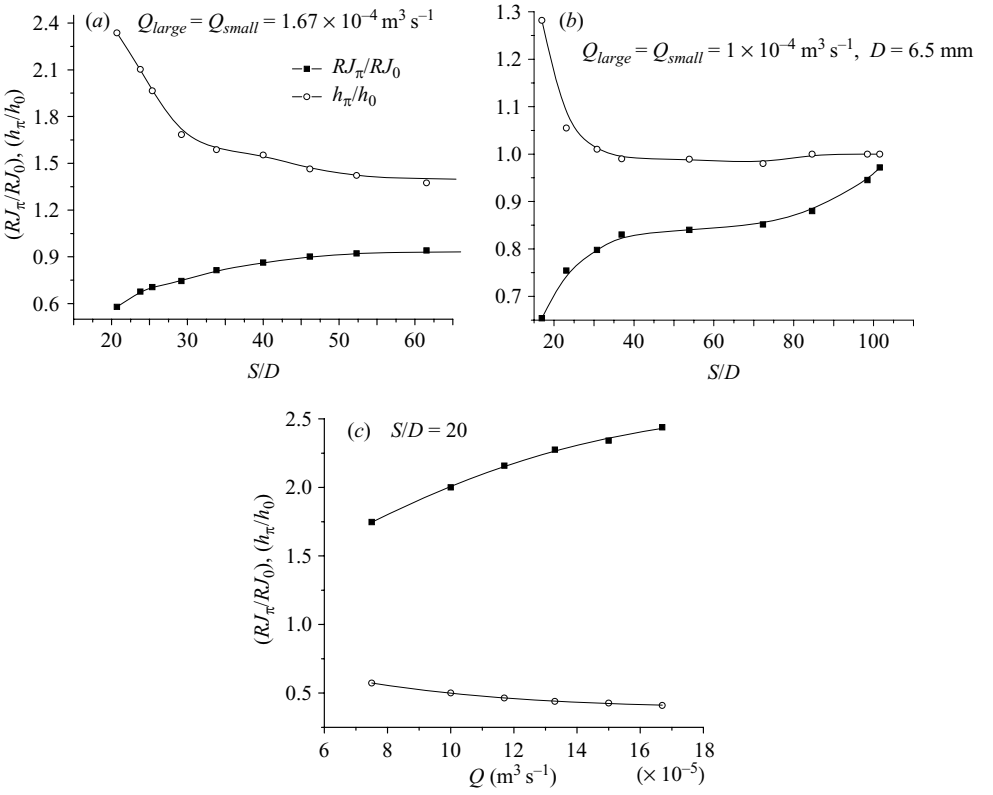

FIGURE 6. Effect of film thickness at the centre of the stagnation line and flow rate on the corresponding. jump location.

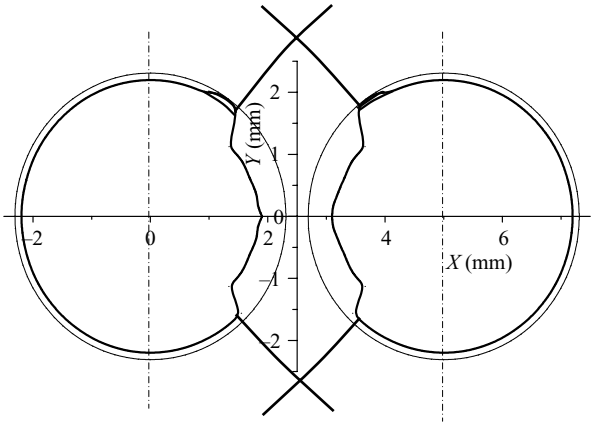

FIGURE 7. Butterfly-shaped hydraulic jump profile ($Q = 1.0 \times 10^{-5}$ m^3 s^{-1}, $S/D = 7.69$, $H/D = 9.23$).

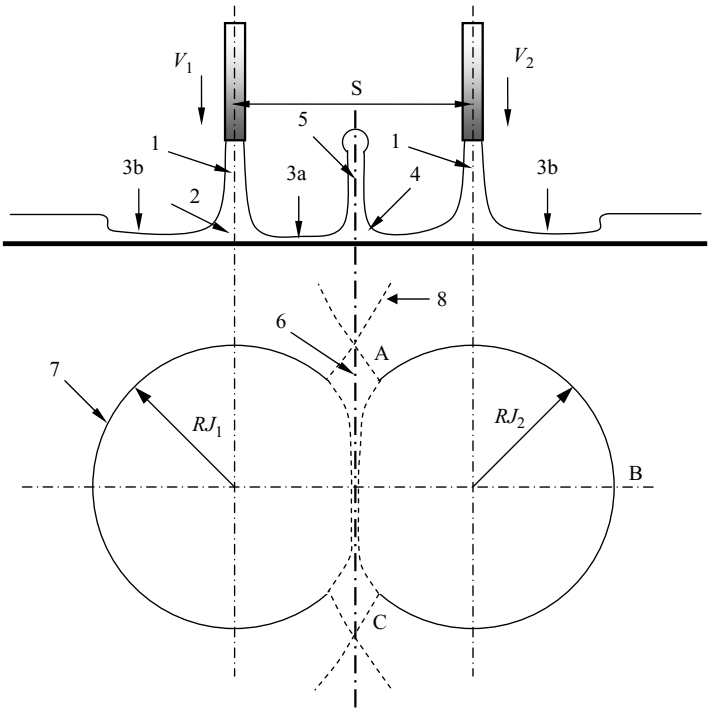

FIGURE 8. Schematic of two adjacent normal impinging liquid circular jets illustrating the main flow characteristics (1. Free jet region, 2. impingement region, 3a. inner wall jet regions, 3b outer wall jet regions, 4. hydraulic jump, 5. wall jet interaction region, 6. influenced jump region, 7. stagnation line, 8. interacting jump segments).

can be observed in the outer wall region. However, in the inner wall jet region, there is a deviation, which can be attributed to the wall jet interactions in that region.

4.2. *Adjacent jets*

When the two impinging jets are spaced such that the distance between them is less than the sum of the radii of the circular hydraulic jumps formed due to single independent jets ($RJ_1 + RJ_2 < S$), the thin films flowing with supercritical velocities in the inner wall region of the two jets collide and give rise to a different flow phenomenon. After undergoing a collision at the stagnation line, the thin films shooting from both the jets take an abrupt 90° turn and emerge as a thin vertical liquid sheet. This is similar to the upwash fountain formation, as reported in the case of twin impinging gas jets and as depicted in figure 2. In the present case, the upwash liquid fountain has the shape of an arch or an approximate segment of a circle formed on a chord which coincides with the stagnation line. The maximum height of this arch lies on the point where line joining the centre of the jet intersects the stagnation line. Though the arch is formed by a thin liquid sheet, its periphery is characterized by a thick rim or crown with an approximately circular cross-section. A cartoon of the flow phenomenon depicting a sectional view through the mid-plane and the top view is shown in figures 8(*a*) and 8(*b*), respectively. The traces of typical interacting jump profiles in the case of adjacent jets are depicted in figure 9, with the jump profiles for single jets are superimposed, for comparison.

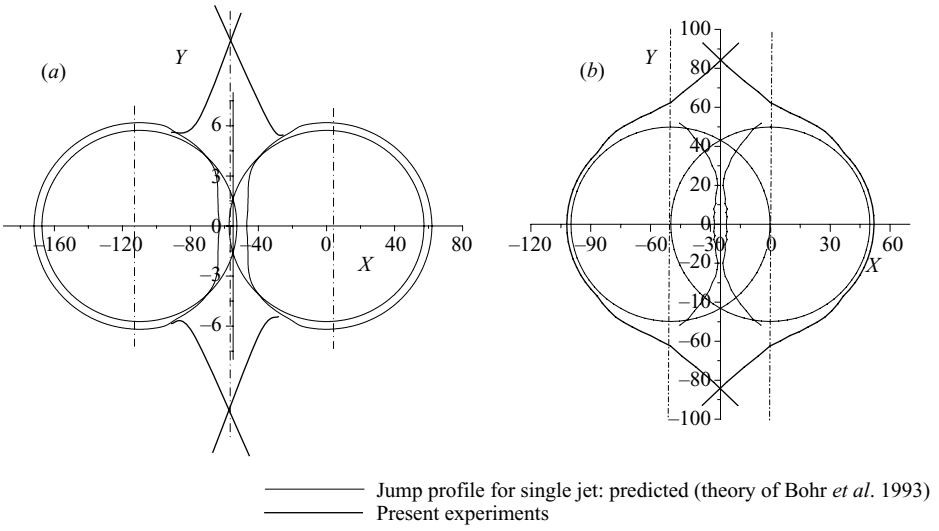

FIGURE 9. Hydraulic jump profiles due to equal adjacent impinging jets: (*a*) $Q = 4.12 \times 10^{-5}$ m ^{3} s^{-1}, $S/D = 16.9$, $H/D = 9.23$; (*b*) $Q = 3.33 \times 10^{-5}$ m^3 s^{-1}, $S/D = 7.69$, $H/D = 9.23$.

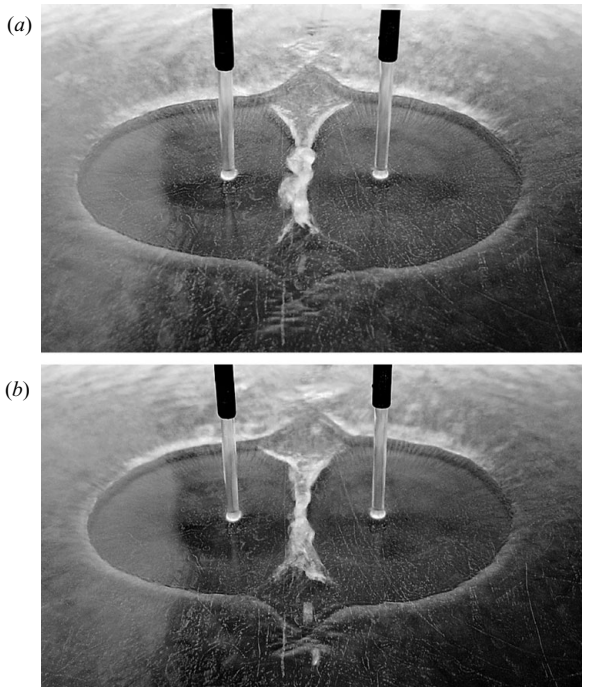

FIGURE 10. (*a*) Begining of upwash formation ($Q = 4.16 \times$, 10^{-5} m^3 s^{-1}, $S/D = 5.17$, $H/D = 10$); (*b*) Fluctuating upwash ($Q = 4.58 \times 10^{-5}$ m^3 s^{-1}, $S/D = 5.17$, $H/D = 10$).

When the jet spacing, S, is nearly equal to $RJ_1 + RJ_2$, the upwash fountain is effectively a fluctuating liquid sheet, as can be seen in figures 10(*a*) and 10(*b*). However, as the jet spacing is reduced, it becomes steady and assumes a well-defined arch shape, as can be seen in figures 11(*a*) and 11(*b*).

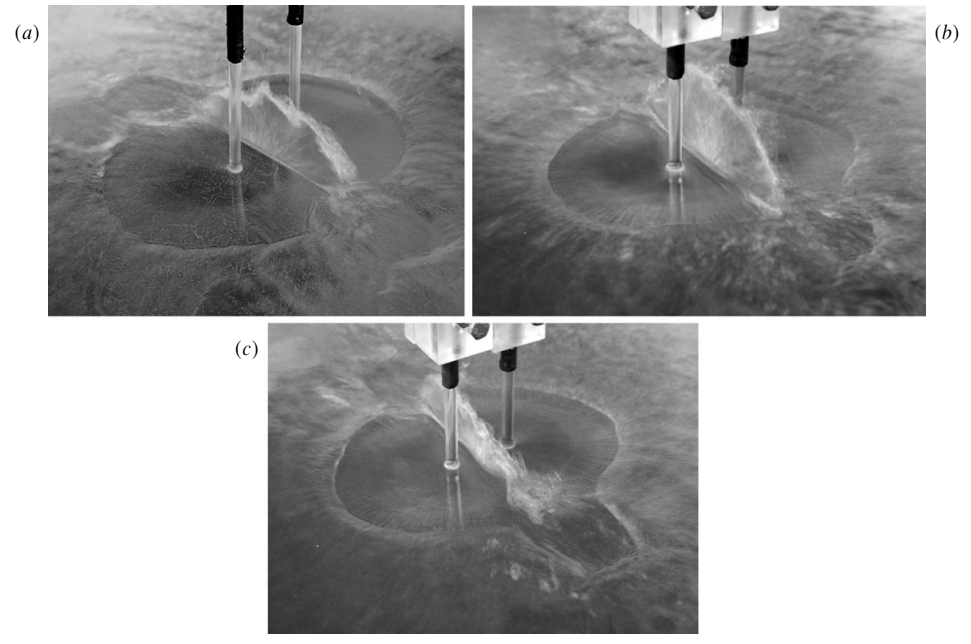

FIGURE 11. Upwash fountain flow ($S/D = 7.69$, $H/D = 10$). (a) Upwash fountain flow, with fluctuating crown ($Q = 1.08 \times 10^{-4}\,\mathrm{m^3\,s^{-1}}$). ($b, c$) Steady upwash fountain flow ($Q = 1.17 \times 10^{-4}\,\mathrm{m^3\,s^{-1}}$).

Flow from the upwash fountain, after reaching the horizontal plane, merges with the radially spreading flow on the plane. At this point, the peripheral flow displaces a segment of the hydraulic jump on the plane and forms obliquely interacting hydraulic jumps (refer to region 8 in figure 8, and figures 9, 10, and 12), similar to those in case of distantly spaced jets, mentioned above. However, for exceptionally close-spaced and high-strength jets, a strong peripheral flow is dominant. This strong flow effectively wipes away the portions of the jump that are located on the horizontal plane in its path, so that intersecting jump segments are observed, as can be seen in figures 11(a) and 11(b). The vertical liquid sheet is considerably thicker for higher values of S, and to be thinner with progressive decreases in S. Air may be trapped at locations where the flow from the upwash fountain mixes again with the thin spreading liquid film. This air eventually escapes in the form of bubbles, as can be seen in the figure 12. The major differences between the flow field associated with the distant and the adjacent impinging jets can be summarized as follows:

(1) In the case of distant impinging jets, the stagnation line region comprises a dome-shaped thick film. However, for adjacent impinging jets, the stagnation line region is a vertical thin liquid sheet.

(2) In the case of distant impinging jets, although the radial symmetry of the hydraulic jump is affected, the jump is identifiable at all the azimuthal locations on the horizontal plate. However, for adjacent impinging jets, the hydraulic jump is visible only within the outer wall jet region (region A-B-C in figure 8).

The fluid flow phenomenon in the arch-shaped upwash (e.g. the spatial spread of the liquid film towards the rim and the return of this flow ultimately to the horizontal target) is not intuitive and is difficult to visualize. However, from the symmetry of the phenomenon, it is not unjustified to assume that an identical flow can be established

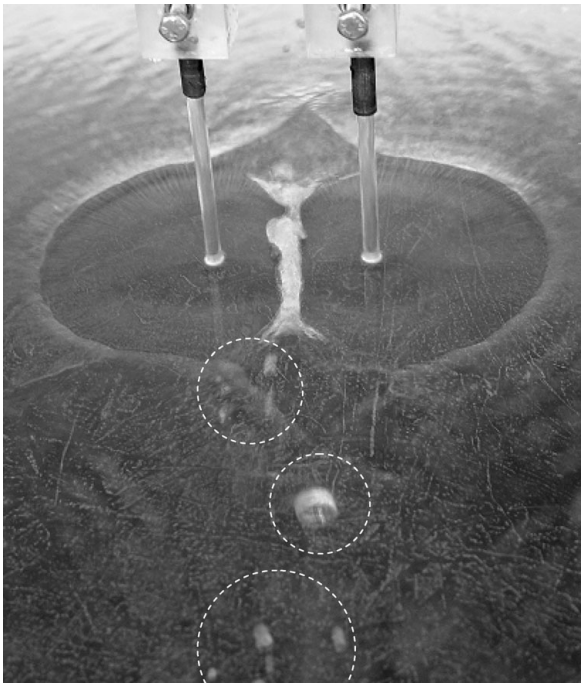

FIGURE 12. Air trapped in two thin sheets in the upwash escapes in the form of air bubbles (encircled).

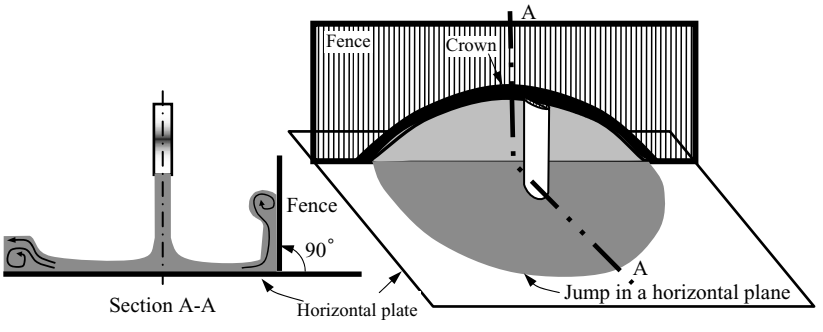

FIGURE 13. Schematic of a single impinging jet with a fenced wall jet.

by a single jet, when a solid vertical wall is placed on the stagnation line. To verify this conjecture, a series of experiments were conducted using a single jet impingement with a vertical fence over the target plate. The observed flow phenomenon (figure 13) was as anticipated.

5. Simulation of flow due to two equal jets using a single jet and a fence

When the circular liquid jet impinges at a point on the horizontal target close to the vertical fence, the hydraulic jump takes the form of a circular segment and ends very close to the fence to form an arch-shaped thin liquid sheet bounded by a thicker rim. Some of the parametric measurements of this phenomenon are elaborated below.

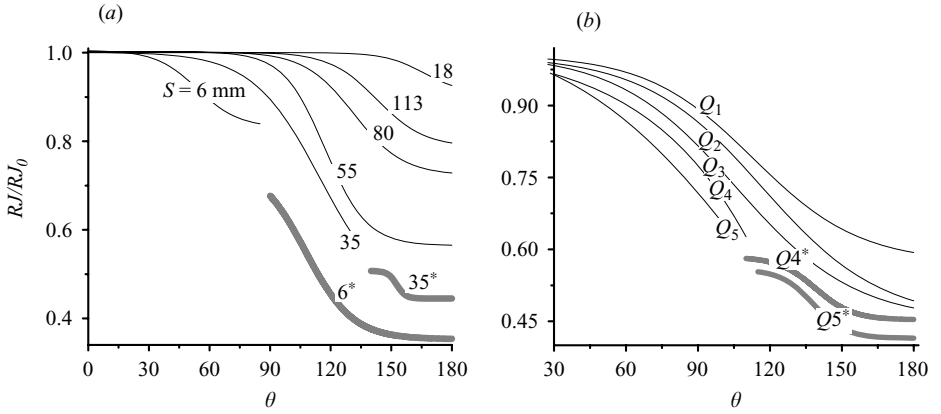

FIGURE 14. Radial locations of the jump due to fenced wall jet (*a*) for a fixed Q ($1.08 \times 10^{-4}\ \mathrm{m^3\ s^{-1}}$) and varying S, and (*b*) for a fixed $S = 22.00$ mm and varying Q ($Q_1 = 1.23 \times 10^{-5}\ \mathrm{m^3\ s^{-1}}$, $Q_2 = 2.5 \times 10^{-5}\ \mathrm{m^3\ s^{-1}}$, $Q_3 = 5.00 \times 10^{-5}\ \mathrm{m^3\ s^{-1}}$, $Q_4 = 8.33 \times 10^{-5}\ \mathrm{m^3\ s^{-1}}$, $Q_5 = 1.00 \times 10^{-4}\ \mathrm{m^3\ s^{-1}}$); * location of the crown on a vertical fence.

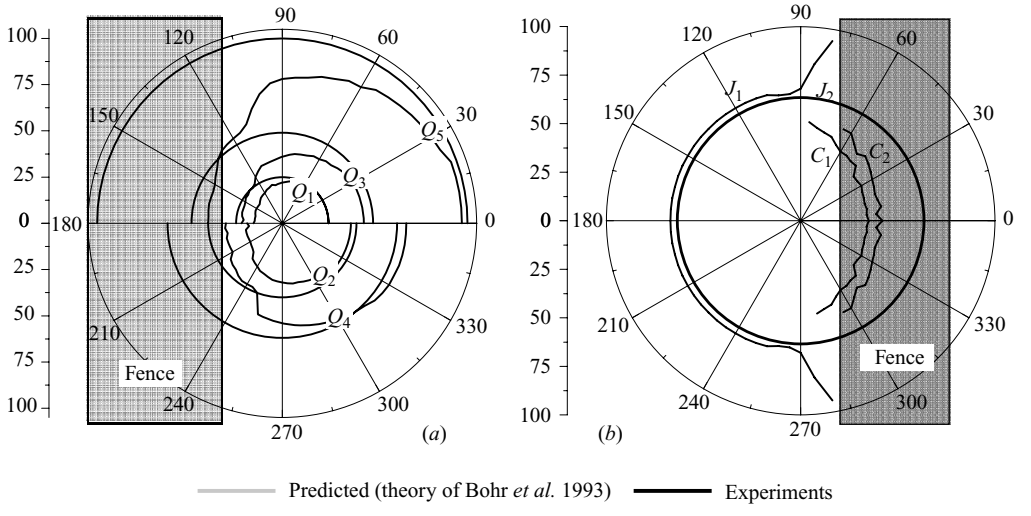

FIGURE 15. Profiles of the hydraulic jump on a horizontal plate and a crown on a vertical fence (*a*) $Q_1 = 1.23 \times 10^{-5}\ \mathrm{m^3\ s^{-1}}$, $Q_2 = 2.5 \times 10^{-5}\ \mathrm{m^3\ s^{-1}}$, $Q_3 = 5.00 \times 10^{-5}\ \mathrm{m^3\ s^{-1}}$, $Q_4 = 8.33 \times 10^{-5}\ \mathrm{m^3\ s^{-1}}$, $Q_5 = 1.00 \times 10^{-4}\ \mathrm{m^3\ s^{-1}}$); (*b*) $Q = 5.00 \times 10^{-5}\ \mathrm{m^3\ s^{-1}}$, $H/D = 9.83$: J – hydraulic jump on the horizontal plate, C_1 – inner edge of the crown, C_2 – outer edge of the crown.

The radial location of the hydraulic jump on the horizontal plate and that of the crown on the vertical plate, for different locations of the jet relative to the fence (here, S is the horizontal distance of the impingment point from the inner surface of a vertical fence), and for different volume flow rates of the liquid, are depicted in figures 14 and 15. They show, radial symmetry of the circular hydraulic jump is influenced that by the fencing of the radial wall jet. Though a portion of the supercritical thin film spreads radially on the vertical fence, its profile is not circular as can be seen from figures 15(*a*) and 15(*b*). Crowns of the thick film formed on the vertical film have definite thicknesses, as can be seen in figure 15(*b*). The maximum

height of the crown on the fence is observed to be less than the corresponding upwash fountain formed in the case of two impinging jets.

For the visualization of up- and downflows in the upwash fountain, the dye injection method is adopted. A number of injection holes (of 0.5 mm diameter) are drilled in the vertical fence. Stainless steel nozzles of matching diameter are attached to these holes from the back side (or dry side) of the fence. A coloured dye can be injected through any of these selected holes, by means of a gravity feed mechanism.

Although a number of flow visualization experiments were conducted, only two important cases are elaborated in this paper to explain the flow phenomenon. The corresponding flow is shown in figure 16. The dye is injected through a hole situated on a line which passes through a plane of symmetry of the upwash fountain (figure 16*a*, *b*). This line is the orthogonal projection of the jet centreline on the vertical fence. As the dye enters the vertical thin film region, it fans out in the form of a radial sector and moves up. The expanding fan of coloured dye is symmetric with respect to its point of origination and continues its upward motion till it reaches the peripheral rim, where the coloured stream bifurcates and flows down from the topmost point (point A, figure 16*b*) of the rim to the horizontal plate along two bifurcations A-B and A-C. This clearly explains the fluid flow in the fountain region, which is characterized by an upward spreading flow through the vertical thin film and then downward flow only through the peripheral rim. To substantiate this observation, dye is injected through another hole situated on a line at an angle β (figure 16*c*, *d*). In this case also, the emerging dye fans out radially, but before it reaches the topmost point of the upwash fountain, it takes a downward path through only the outer rim. However, it does not bifurcate and takes the shortest path along the periphery from its topmost point of ascent.

6. Upwash fountain flow

From the flow visualization experiments with a single jet and a fence, as described in § 5, it can be concluded that the upwash liquid fountain for the adjacent liquid jets is formed due to a 90° turn of thin horizontal liquid films. The upflow of the liquid is characterized by radial spreading from the stagnation line, while the downward flow is only through the peripheral rim of the upwash fountain. A sketch is given in figure 17. It is interesting to note that though a fan-shaped coloured stream is clearly identifiable in the thin film region of the upwash (once it reaches the rim region), as can be seen in figure 16(*a*), the dye is thoroughly mixed and the colour appears in the entire rim region. As the rim region is continuously fed with liquid coming from all the points of the periphery, good mixing in this region is likely.

It is important to note in this context that the formation of a thin liquid sheet due to the collision of two free jets has been observed in a number of other studies (Taylor 1960; Hasson & Peck 1964; Choo & Kang 2001, 2002; Bush & Hasha 2004; Bremond & Villermaux 2006). When two circular free liquid jets collide obliquely in a vertical plane, the liquid expands radially from the point of impact, forming a thin film, in the form of bay leaf (Bremond & Villermaux 2006). Radially expanding liquid is collected in the thick peripheral rim, which bounds the thin liquid sheet. Ultimately, the liquid drains through the rim at the bottommost point of the leaf-like structure.

The arch-shaped upwash fountain that is observed in the present work represents a phenomenon similar to the impingement of two free jets. However, it may be noted that in the case of free jets, the impingement zone virtually converges to a point

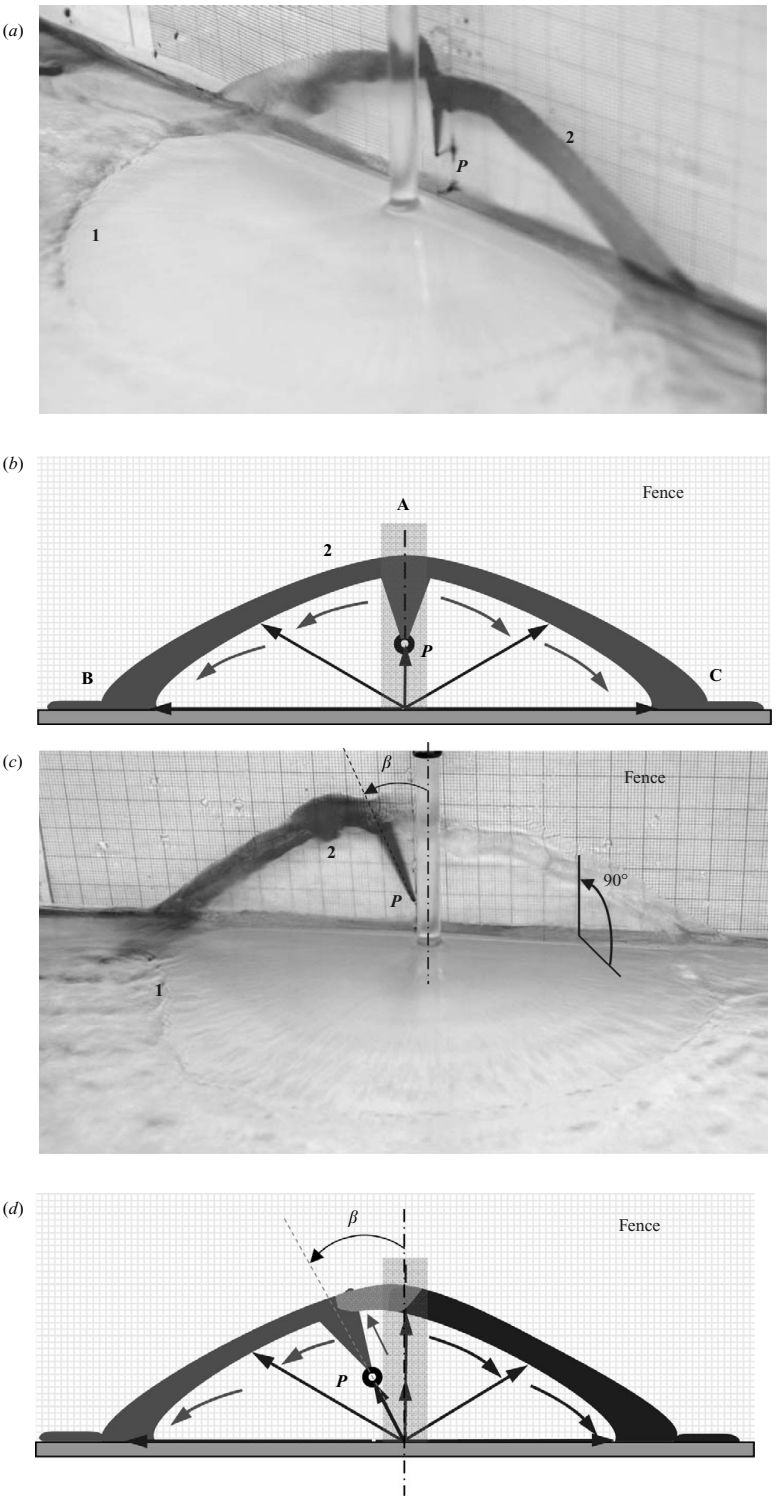

FIGURE 16. A typical single impinging jet with a fenced wall jet (P is the dye injection point, 1 and 2 indicate hydraulic jump and thick crown in horizontal and vertical planes respectively): $Q = 1.08 \times 10^{-4}$ m^3 s^{-1}, $H/D = 9.82$, $S/D = 1.03$. (a, b) Dye injected through plane of symmetry of upwash region, (c, d) dye injected at angle β.

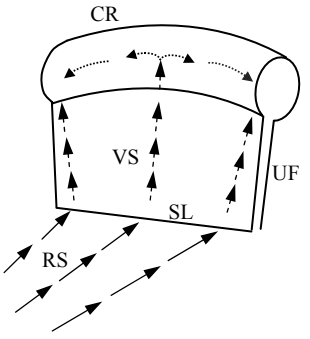

FIGURE 17. Schematic of a section of an upwash fountain flow: RS – radially spreading flow, SL – stagnation line, VS – vertically spreading flow, UF – upwash fountain, CR – crown.

(or a small elliptical region). On the other hand, in the present case, the liquid films in the form of two opposing wall jets collide with each other to form the vertical sheet. Moreover, the liquid spreading in the vertical sheet is collected in the peripheral rim.

7. Effect of hydraulic jump interactions on the jump profiles

A typical hydraulic jump profile for distant impinging jets is sketched in figure 7, and for adjacent impinging jets in figure 9. The corresponding hydraulic jump profiles captured during our laboratory experiments are depicted in figure 8(*b*) for the case of distant impinging jets, and in figures 10, 11, and 12 for the cases of adjacent impinging jets. As can be seen in these figures, the radial symmetry of the hydraulic jumps is disturbed due to opposing wall jet interactions, conferring non-circular shapes on the hydraulic jumps in all cases.

Effects of volume flow rate of liquid (keeping the jet spacing fixed) on the radial locations of the jump are depicted in figure 18. The effects of jet spacing (keeping the volume flow rates unaltered) are depicted in figure 19. As can be seen from these figures, the ratio RJ_θ/RJ_π is equal to 1, for all values of θ (where θ is the azimuthal location), for the far-distant impinging jets (figure 18 and figure 19). However, it is less than unity within a portion of the inner wall jet region. The influence of the jump interactions is more pronounced in the case of adjacent impinging jets, than for distant impinging jets as can be seen in figures 18(*c*) to 18(*f*) and figure 19. Here, it is important to note that for adjacent jets, the distance between the jet centre and the upwash fountain has been taken for drawing the curves. This distance basically denotes the spread of the thin liquid film in the horizontal plane, since no hydraulic jump exists within inner wall region on the horizontal plate. Reductions in the jet spacing or increments in the volume flow rate have similar effects on hydraulic jump profiles, as can be seen from figures 18 and 19.

8. Two unequal jets

After performing extensive experiments with two equal jets, we performed a few experiments with two unequal jets. The resultant hydraulic jump interaction patterns were similar to those formed with two equal interacting jets. The critical jet spacing, as a function of volume flow rates of the liquid, is shown in figure 20. As can be seen, critical spacing decreases as the ratio Q_{large}/Q_{small} (where Q_{large} and Q_{small} are the volume flow rates of liquid through the large and the small jets, respectively) increases.

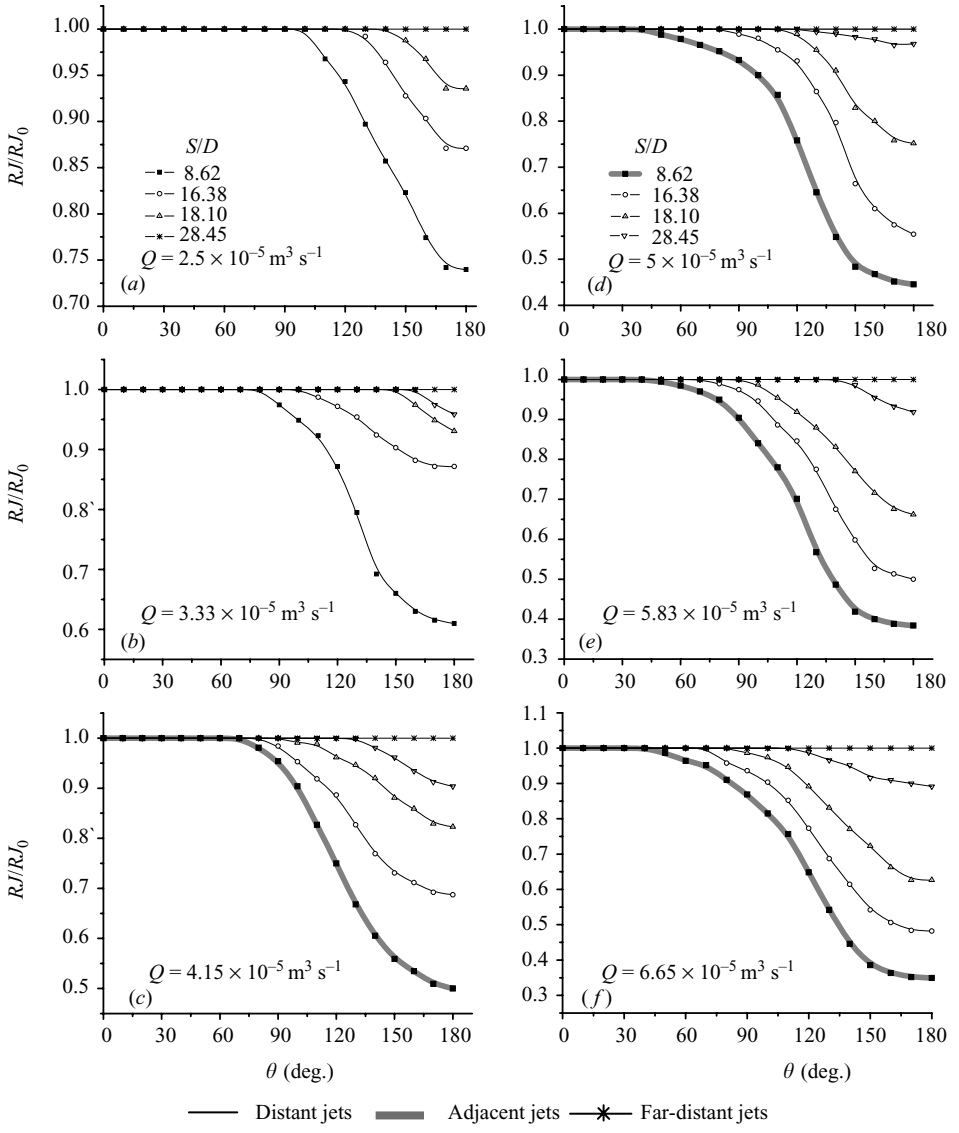

FIGURE 18. Effect of interactions of the jump on radial locations of the jump for different jet spacings: relatively less jump region is influenced for distant impinging jets in comparison with adjacent impinging jets.

Typical jump profiles for two unequal impinging jets are depicted in figures 21 and 22. The only remarkable difference with the case of equal impinging jets is that the stagnation line is curved, and the upwash fountain is not perpendicular to the target plate. Rather, it is curved and inclined towards the smaller jet, as can be seen in figure 23. As mentioned earlier, the location of the stagnation line depends on the strength of the individual jets. The wall jet interactions, in such cases, give rise to curved stagnation lines that are located nearer to the relatively weaker jet, as can be seen in figure 21(*a*). Locations of the stagnation line, as predicted using (1.1) and as measured during our experiments (along the line joining the centres of the two jets), are depicted in figure 24. Radial locations of the jump, with changes in the volume

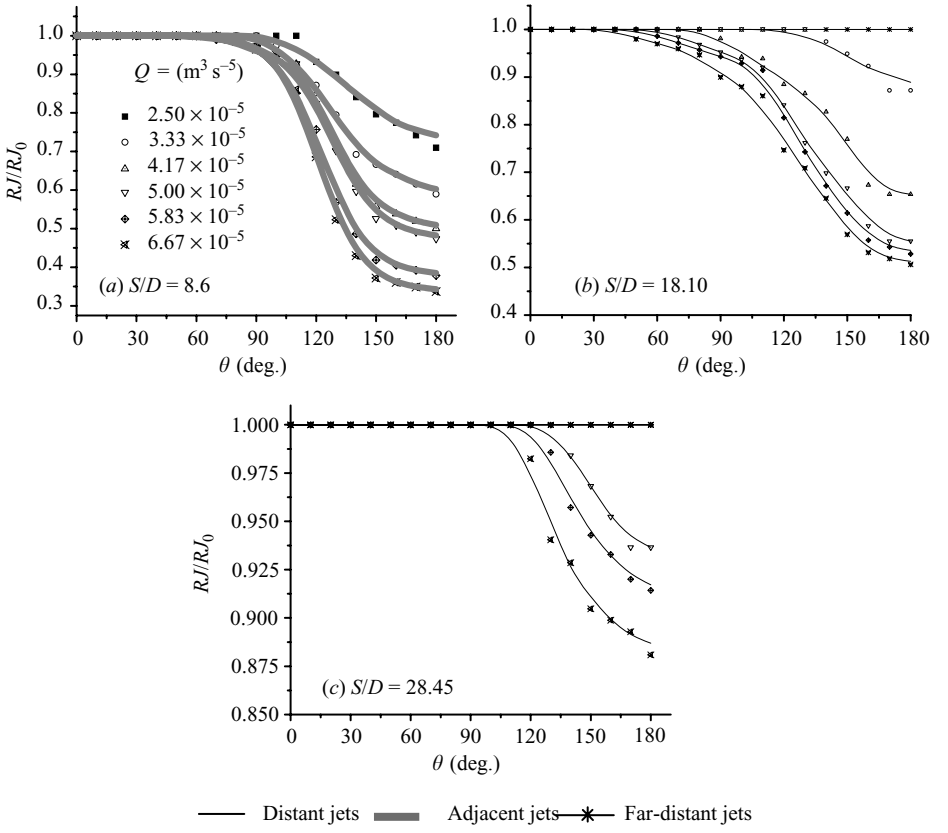

FIGURE 19. Effect of interactions of the jump on radial locations of the jump for different volume rates of liquid.

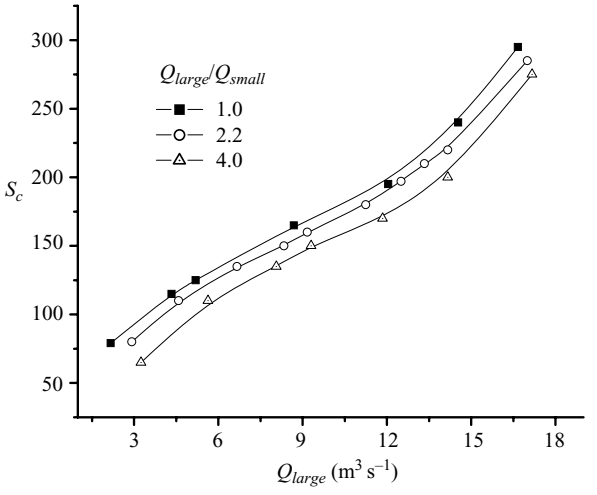

FIGURE 20. Critical spacing for jets of unequal strength.

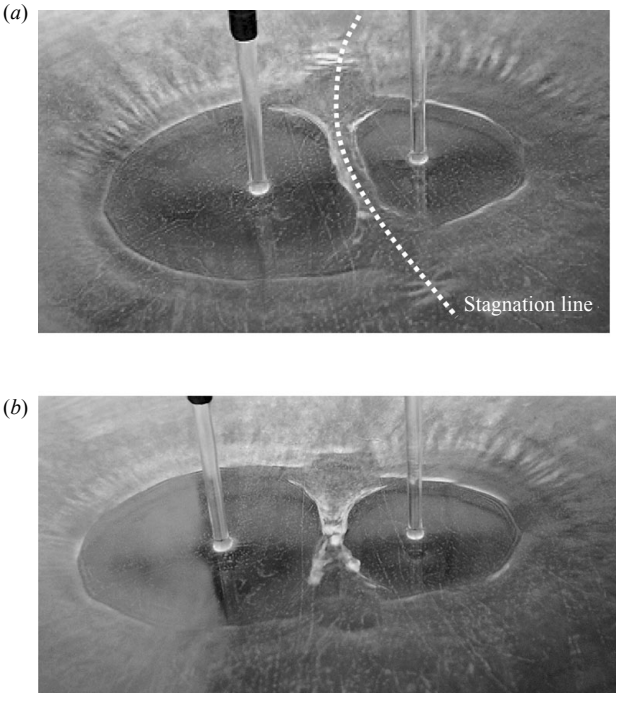

FIGURE 21. Hydraulic jump profiles in the case of two unequal impinging jets: $Q_{large} = 5.83 \times 10^{-5}$ m^3 s^{-1}, $Q_{small} = 2.5 \times 10^{-5}$ m^3 s^{-1}, $H/D = 11.20$, (*a*) $S/D = 10.34$, (*b*) $S/D = 8.62$.

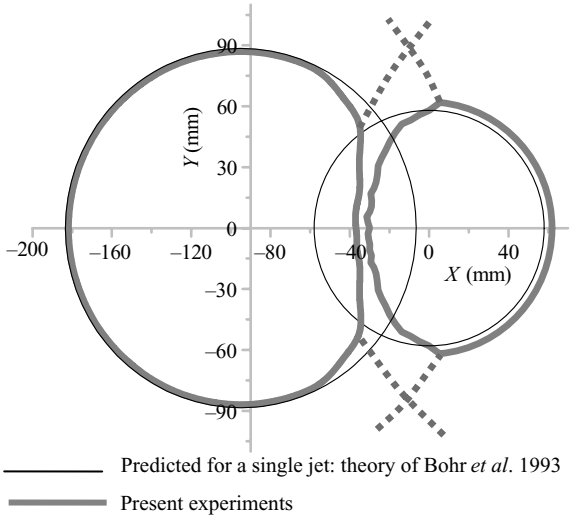

FIGURE 22. Hydraulic jump profile in the case of two unequal impinging normal jets: $Q_{large} = 9.17 \times 10^{-5}$ m^3 s^{-1}, $Q_{small} = 5 \times 10^{-5}$ m^3 s^{-1}.

flow rate of liquid and the jet spacings, are depicted in figures 25(*a*) to 25(*e*). As can be seen in these figures, hydraulic jump profiles due to the smaller jet are influenced more severely than those due to the larger jets, as a consequence of interactions between the two jumps.

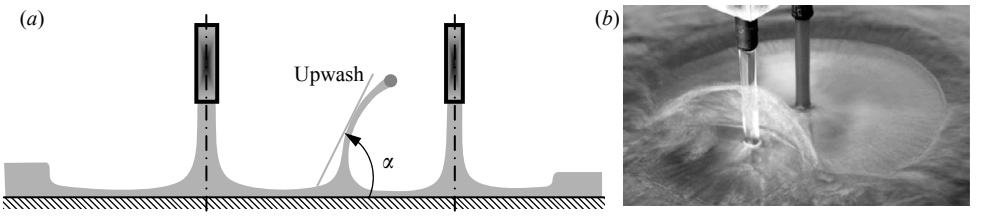

FIGURE 23. Two adjacent impinging jets with inclined upwash: (*a*) schematic representation; (*b*) inclined upwash during laboratory experiments.

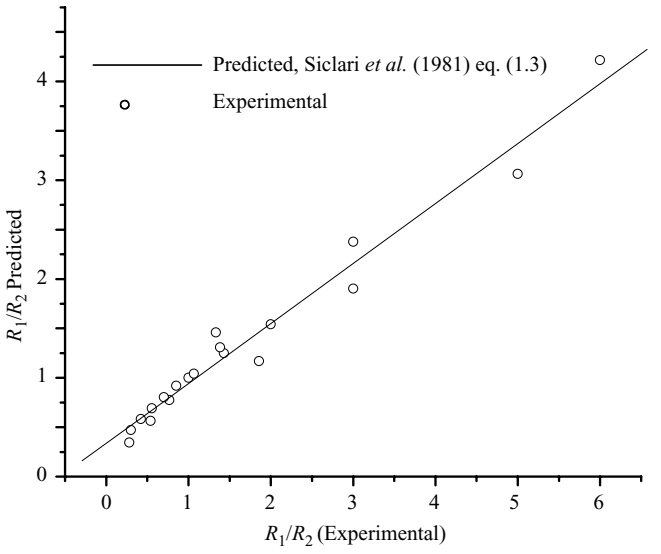

FIGURE 24. Location of the stagnation line.

Although the hydraulic jumps due to the smaller jets are more influenced by wall jet interactions of unequal jets, each jump has a distinctive visual appearance. A typical case of interacting jump profiles due to unequal impinging jets occurs when the difference of the flow rates between the two individual jets become progressively greater (figure 26*a*). Under these conditions, the hydraulic jump due to the smaller jet disappears altogether in the jump region of the larger jet. Typical hydraulic jump profiles under these conditions are depicted in figure 27(*a*). A portion of the hydraulic jump formed due to the larger jet is seen to be influenced due to the smaller jet. The influenced section of the jump profile is concave at a relatively low volume flow rate of the smaller jet, as can be seen in figure 26(*a*). With increase in the flow rate of the smaller jet, the influenced jump profile becomes to a straight line and with further increase in the flow rate of the smaller jet it becomes convex, as can be seen in figures 26(*b*) and 27(*a*). The radial locations of the jump formed due to the larger jet, for different inter-jet spacings are depicted in figure 27(*b*).

9. Conclusions

A comprehensive study on the spreading flow due to the normal impingement of two closely spaced liquid jets has been reported. The interaction between two

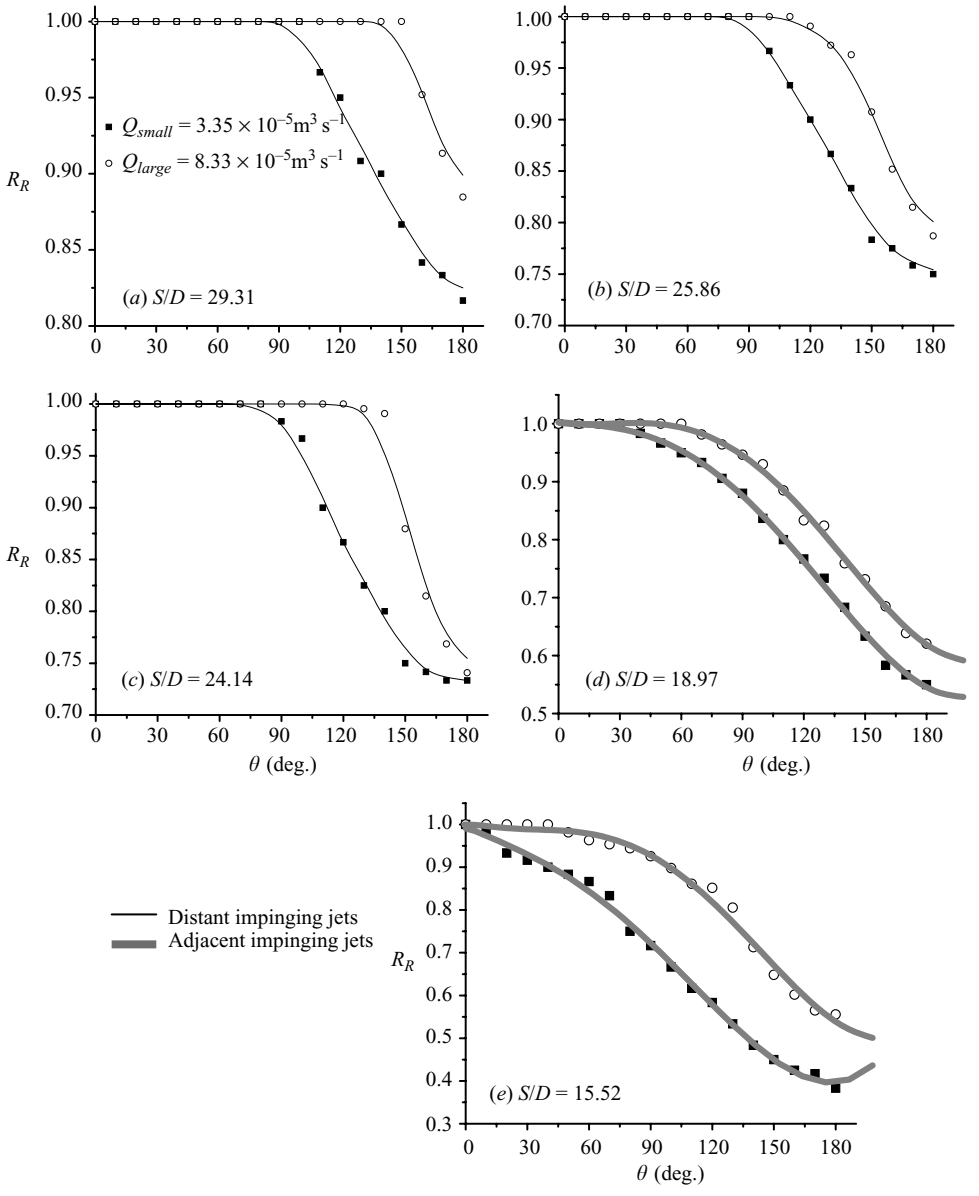

FIGURE 25. Radial locations of the jump due to unequal impinging jets.

impinging air jets submerged in an ambient medium of air has been studied earlier in connection with VTOL aircrafts. In such systems, a strong entrainment of the ambient air into the jet plumes and spreading wall jets creates a sub-atmospheric pressure known as 'suckdown'. When the spreading wall jets from two impinging propulsion jets meet, they turn upward, with a relatively narrow sheet of flow (similar to a two-dimensional jet but spreading faster and having a three-dimensional structure). This flow is referred to as an upwash. However, the interaction between the spreading flow from two impinging liquid jets and the associated upwash formation had not been reported prior to this study.

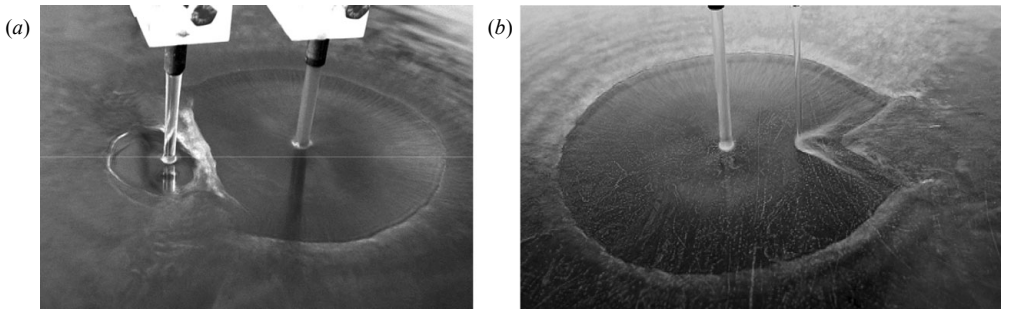

FIGURE 26. Typical hydraulic jump profiles due to two unequal (excessively large momentum ratio) impinging jets: (*a*) $Q_{large} = 1.00 \times 10^{-4}$ m^3 s^{-1}, $Q_{small} = 2.13 \times 10^{-5}$ m^3 s^{-1}; (*b*) $Q_{large} = 1.33 \times 10^{-4}$ m^3 s^{-1}, $Q_{small} = 1.65 \times 10^{-5}$ m^3 s^{-1}.

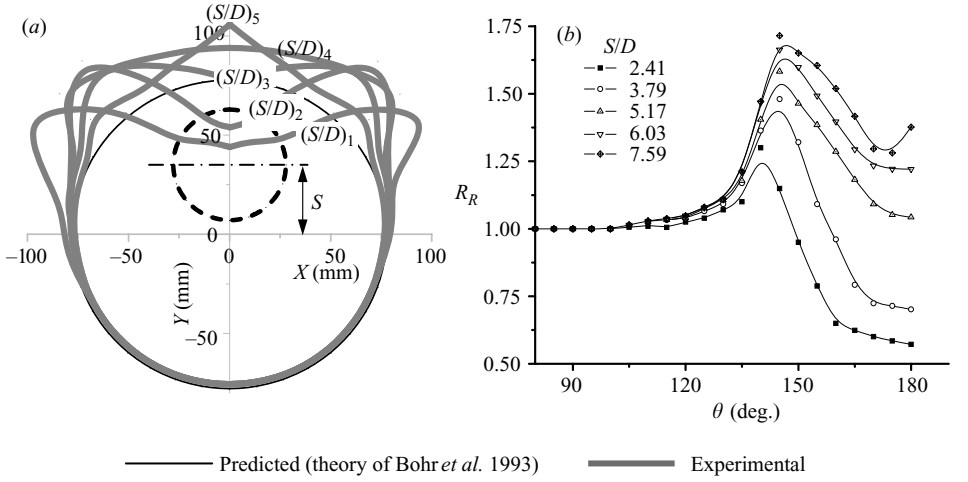

FIGURE 27. (*a*) Plot showing jump profile in the case of excessively unequal jets: $(S/D)_1 = 2.41$, $(S/D)_2 = 3.79$, $(S/D)_3 = 5.17$, $(S/D)_4 = 6.03$, $(S/D)_5 = 7.59$, (*b*) Radial location of jump due to the larger jet for different jet spacing. $Q_{large} = 9 \times 10^{-5}$ m^3 s^{-1}, $Q_{small} = 1 \times 10^{-5}$ m^3 s^{-1}.

The upwash formation due to two closely spaced impinging liquid jets shows a remarkable difference with the upwash formed by submerged air jets. There are two main reasons for this difference. In the case of submerged air jets, there is a substantial entrainment from the ambient medium both into the thin film region and into the upwash region. Such a strong entrainment is absent when liquid jets are impinging on a solid surface. The formation of hydraulic jumps and the interaction between the jumps in the case of liquid jets is unique phenomenon, which is absent in an air–air system. The interaction between the hydraulic jumps gives rise to a series of complex hydrodynamic phenomena and creates interesting jump–jump interaction patterns.

The interaction between the twin jets can be categorized into three different types, depending on the distance between them. When the jets are far apart (far distant), the jump profiles remain almost unaltered. As they move closer, the individual jumps start exhibiting non-circular profiles, with a clear stagnation line demarcating the flows emerging from each of the jets. This is a straight line for equal jets, and a curved one for unequal jets. When the spacing between the jets is below a critical limit, an upwash fountain is observed on a stagnation line. The upwash fountain is

an arch-shaped sheet of liquid bounded by a thick rim. Again, it is straight for two equal jets and is bent towards the smaller jet when the two jets are not identical.

The critical spacing for the jump–jump interactions to take place has also been reported in this study. Systems of two impinging jets have been classified into three groups, namely, far-distant impinging jets, distant impinging jets and adjacent impinging jets. Non-circular hydraulic jump profiles due to jump–jump interactions have been investigated for these distinctive cases, both for equal and unequal impinging jets. Film thicknesses have been measured at the centre of the stganation line. The effect of film thickness on the corresponding jump locations has been reported.

Flow pattern due to two equal impinging jets have, finally, been simulated by using a single jet and a fence, for more convenient visualization of upwash fountain flow. The fluid from the opposing thin films takes a 90° turn and forms a vertical upwash zone after collision. The flow in the upwash zone is mainly radial. The fluid comes back to the horizontal target plate through a thick rim formed at the periphery of the upwash. The phenomenon of the upwash fountain and the formation of the peripheral rim are similar to the development of thin spreading sheet due to the impact of two free liquid jets.

REFERENCES

Adarkar, D. B. & Hall, G. R. 1969 The 'fountain effect' and VTOL exhaust ingestion. *J. Aircraft* **6**, 109.

Arakeri, J. H. & Rao, A. 1996 On radial flow on a horizontal surface and the circular hydraulic jump. *J. Indian Inst. Sci.* **76**, 73–91.

Aristoff, J. M., Leblanc, J. D., Hosoi, A. E. & Bush, J. W. M. 2004 Viscous hydraulic jumps. *Phys. Fluids* **16**, S4.

Barata, J. M. M. 1996 Fountain flows produced by multiple impinging jets in a crossflow *AIAA J.* **34**, 2523–2530.

Beltos, S. 1976 Oblique impingement of circular turbulent jets. *J Hydraul. Res.* **14** 17–36.

Blackford, B. L. 1996 The hydraulic jump in radially spreading flow: A new model and new experimental data. *Am. J. Phys.* **64**, 164–169.

Bohr, T., Dimon, P. & Putkaradze, V. 1993 Shallow-water approach to the circular hydraulic jump. *J. Fluid Mech.* **254**, 635–648.

Brechet, Y. & Néda, Z, 1999 On the circular hydraulic jump. *Am. J. Phys.* **67**, 723–731.

Bremond, N. & Villermaux, E. 2006 Atomization by jet impact. *J. Fluid Mech.* **549**, 273–306.

Bush, J. W. M. & Aristoff, J. M. 2003 The influence of surface tension on the circular hydraulic jump. *J. Fluid. Mech.* **489**, 229–238.

Bush, J. W. M., Aristoff, J. M. & Hosoi, A. E. 2006 An experimental investigation of the stability of the circular hydraulic jump. *J. Fluid. Mech.* **558**, 33–52.

Bush, J. W. M. & Hasha, A. E. 2004 On the collision of laminar jets: fluid chains and fishbones. *J. Fluid. Mech.* **511**, 285–310.

Cabrita, P. M., Saddington, A. J. & Knowles, K. 2005 PIV measurements in a twin-jet STOVL fountain flow. *Aeronaut. J.* **109**, 439–449.

Choo, Y. J. & Kang, B. S. 2001 Parametric study on impinging-jet liquid sheet thickness distribution using an interferometric method. *Exps. Fluids* **31**, 56–62.

Choo, Y. J. & Kang, B. S. 2002 The velocity distribution of the liquid sheet formed by two low-speed impinging jets. *Phys. Fluids* **14**, 622–627.

Craik, A., Lathman, R., Fawkes, M. & Gibbon, P. 1981 The circular hydraulic jump. *J. Fluid. Mech.* **112**, 347–362.

Elbanna, H. & Sabbagh, J. A. 1989 Flow visualization and measurements in a two-dimensional two-impinging-jet flow. *AIAA J.* **27**, 420–426.

Ellegaard, C., Hansen, A. E., Hanning, A., Hansen, K., Marcussen, A., Bohr, T., Hansen, J. L. & Watanabe, S. 1998 Creating corners in kitchen sinks. *Nature* **392**, 767–768.

Ellegaard, C., Hansen, A. E., Hanning, A., Hansen, K., Marcussen, A., Bohr, T., Hansen, J. L. & Watanabe S. 1999 Cover illustration: Polygonal hydraulic jumps. *Nonlinearity* **12**, 1–7.

Gilbert, B. 1989 Turbulence measurements in a radial upwash. *AIAA J.* **27**, 44–51.

Godwin, R. 1993 The hydraulic jump ("shocks" and viscous flow in the kitchen sink). *Am. J. Phys.* **61**, 829–832.

Hamed, M. S. & Akmal, M. 2005 Determination of heat transfer rates in an industry-like spray quench system using multiple impinging water jets. *Intl J. Materials Product Technol.* **24**, 184–198.

Hansen, S. H., Horlúck, S., Zauner, D., Dimon, P., Ellegaard, P. & Watanabe, S. 1997 Geometrical orbits of surface waves from a circular hydraulic jump. *Phy. Rev.* E **55**, 7048–7061.

Hasson, D. & Peck, R. E. 1964 Thickness distribution in a sheet formed by impinging jets. *AIChE J.* **10**, 752–754.

Hill Jr., W. G. 1985 Effects of a central fence on upwash flows. *J. Aircraft* **22**, 771–775.

Hill Jr., W. G. & Jenkins, R. C. 1980 Effect of nozzle spacing on ground interference forces for a two-jet V/STOL aircraft. *J. Aircraft* **17**, 684–689.

Higuera, F. J. 1994 Hydraulic jump in a viscous laminar flow. *J. Fluid Mech.* **274**, 69–92.

Higuera, F. J. 1997 The circular hydraulic jump. *Phys. Fluids* **9**, 1476–1478.

Ishigai, S., Nakanishi, S., Mizunao, M. & Imamura, T. 1977 Heat transfer of the impinging round water jet in the interference zone of film flowing along the wall. *Bull. JSME* **20**, 85–92.

Kate, R. P., Das, P. K. & Chakraborty, S. 2007*a* Hydraulic jumps due to oblique impingement of circular liquid jets on a flat horizontal plate. *J. Fluid Mech* **573**, 247–263.

Kate, R. P., Das, P. K. & Chakraborty, S. 2007*b* Hydraulic jumps with corners due to obliquely inclined circular liquid jets. *Phys. Rev.* E **75**, 056310-1–056310-6.

Kind, R. J. & Suthanthiran, K. 1972 The interaction of two opposing plane turbulent wall jets. *AIAA Paper* 72-211.

Lienhard V, J. H. 2006 Heat transfer by impingement of circular free-surface liquid jets. *18th National and 17th ISHMT-ASME Conference IIT Guwahati, India*, pp. k206–k221.

Liu, X. & Lienhard V, J. H. 1993*a* Extremely high heat fluxes beneath impinging jets. *J. Heat Transfer* **115**, 472–476.

Liu, X. & Lienhard V, J. H. 1993*b* The hydraulic jump in circular jet impingement and in other thin. liquid films. *Exps. Fluids* **15**, 108–116.

Miller, P. 1995 A study of wall jets resulting from single and multiple inclined jet impingement *Aeronaut. J.* **32**, 201–216.

Nakoryakov, V., Pokusaev, B. & Troyan, E. 1978 Impingement of an axisymmetric liquid jet on a barrier *Intl J. Heat Mass Transfer* **21**, 1175–1184.

Olsson, R. G. & Turkdogan, E. T. 1966 Radial spread of a liquid stream on a horizontal plate. *Nature* **211**, 813–816.

Rao, A. & Arakeri, J. H. 1998 Integral analysis applied to radial film flows. *Intl J. Heat Mass Transfer* **41**, 2757–2767.

Rubel, A. 1981 Computations of the oblique impingement of round jets upon a plane wall. *AIAA J.* **19**, 863–871.

Rubel, A. 1982 Oblique impingement of a round jet on plane surface. *AIAA J.* **20**, 1756–1758.

Saripalli, K. R. 1983 Visualization of multijet impingement flow. *AIAA J.* **21**, 483–484.

Siclari, M. J., Aidala, P., Wohllebe, F. & Palcza, J. L. 1977 Development of prediction techniques for multi-jet thermal ground flow field and fountain formation. *AIAA Paper* 77-616.

Siclari, M. J., Hill Jr., W. G. & Jenkins, R. C. 1981 Stagnation line and upwash formation of two impinging jets. *AIAA J.* **19**, 1286–1293.

Siclari, M. J., Migdal, D. & Luzzi Jr., T. W. 1976 Development of theoretical models for jet-induced effects on V/STOL aircraft. *J. Aircraft* **13**, 938–944.

Skifstad, J. G. 1970 Aerodynamics of jets pertinent to VTOL aircraft. *J. Aircraft* **7**, 193–204.

Sparrow, E. M. & Lovell, B. J. 1980 Heat transfer characteristics of an obliquely impinging circular jet. *Trans. ASME: J. Heat Transfer* **102**, 202–209.

Stevens, J. & Webb, B. W. 1991 The effect of inclination on local heat transfer under an axisymmetric free liquid jet. **34**, 1227–1236.

Taylor, G. I. 1960 Formation of thin flat sheets of water. *Proc. R. Soc. Lond.* **259**, 1–17.

Thielen, L., Jonker, H. J. J. & Hanjalic, K. 2003 Symmetry breaking of flow and heat transfer in multiple impinging jets *Intl J. Heat Mass Transfer* **24**, 444–453.

Tong, A. Y. 2003 On the oblique impingement heat transfer of an oblique free surface plane jet. *J. Heat Mass Transfer* **46**, 2077–2085.

Watson, E. J. 1964 The spread of a liquid jet over a horizontal plane. *J. Fluid Mech.* **20**, 481–499.

Yokoi, K. & Xiao, F. 2002 Mechanism of structure formation in circular hydraulic jumps: Numerical studies of strongly deformed free-surface shallow flows. *Physica* D **161**, 202–219.